



UNIVERSIDADE ESTADUAL DE CAMPINAS
SISTEMA DE BIBLIOTECAS DA UNICAMP
REPOSITÓRIO DA PRODUÇÃO CIENTÍFICA E INTELLECTUAL DA UNICAMP

Versão do arquivo anexado / Version of attached file:

Versão do Editor / Published Version

Mais informações no site da editora / Further information on publisher's website:

<https://academic.oup.com/jge/article/15/1/261/5112884>

DOI: 10.1088/1742-2140/aa99f4

Direitos autorais / Publisher's copyright statement:

©2018 by Oxford University Press. All rights reserved.

DIRETORIA DE TRATAMENTO DA INFORMAÇÃO

Cidade Universitária Zeferino Vaz Barão Geraldo

CEP 13083-970 – Campinas SP

Fone: (19) 3521-6493

<http://www.repositorio.unicamp.br>

Probabilistic seismic history matching using binary images

Alessandra Davolio¹ and Denis Jose Schiozer

University of Campinas, Campinas, Brazil

E-mail: davolio@cepetro.unicamp.br and denis@cepetro.unicamp.br

Received 13 June 2017, revised 23 October 2017

Accepted for publication 13 November 2017

Published 23 January 2018



CrossMark

Abstract

Currently, the goal of history-matching procedures is not only to provide a model matching any observed data but also to generate multiple matched models to properly handle uncertainties. One such approach is a probabilistic history-matching methodology based on the discrete Latin Hypercube sampling algorithm, proposed in previous works, which was particularly efficient for matching well data (production rates and pressure). 4D seismic (4DS) data have been increasingly included into history-matching procedures. A key issue in seismic history matching (SHM) is to transfer data into a common domain: impedance, amplitude or pressure, and saturation. In any case, seismic inversions and/or modeling are required, which can be time consuming. An alternative to avoid these procedures is using binary images in SHM as they allow the shape, rather than the physical values, of observed anomalies to be matched. This work presents the incorporation of binary images in SHM within the aforementioned probabilistic history matching. The application was performed with real data from a segment of the Norne benchmark case that presents strong 4D anomalies, including softening signals due to pressure build up. The binary images are used to match the pressurized zones observed in time-lapse data. Three history matchings were conducted using: only well data, well and 4DS data, and only 4DS. The methodology is very flexible and successfully utilized the addition of binary images for seismic objective functions. Results proved the good convergence of the method in few iterations for all three cases. The matched models of the first two cases provided the best results, with similar well matching quality. The second case provided models presenting pore pressure changes according to the expected dynamic behavior (pressurized zones) observed on 4DS data. The use of binary images in SHM is relatively new with few examples in the literature. This work enriches this discussion by presenting a new application to match pressure in a reservoir segment with complex pressure behavior.

Keywords: 4D seismic, seismic history matching, binary images, reservoir simulation

(Some figures may appear in colour only in the online journal)

1. Introduction

4D seismic (4DS) surveys play an increasingly important role in monitoring hydrocarbon reservoirs. The acquired data provide spatial information about the dynamic changes that occur due to production. This information is used to update reservoir simulation models, increasing production forecast reliability, therefore improving field management. Reservoir simulation and 4DS data can be integrated in several ways,

from qualitative assessment (Osdal *et al* 2006, Huang *et al* 2013) to quantitative use in history-matching procedures (Landa and Kumar 2011, Emerick 2016, and Leeuwenburgh and Arts 2014). Integration remains a challenge, especially for the latter. To include 4DS data as part of a history-matching procedure, it is necessary to define a common domain so that seismic data and simulation results can be compared. Ideally, this integration is performed in the pressure and saturation domains as these are prompt results from reservoir simulation. However estimating actual values of pressure and saturation from seismic data is difficult although

¹ Author to whom any correspondence should be addressed.

there are some possibilities such as Tura and Lumley (1999), Landrø (2001) and Trani *et al* (2011). Therefore, the most common domain is the elastic attributes, such as impedance, which can be seen as a halfway point between the forward modeling from simulation results and seismic inversion. The computation of seismic impedances from simulation models is very straightforward; requiring only a forward modeling, performed through a petro-elastic model. Although this is a relatively inexpensive procedure, petro-elastic models can be highly uncertain and the calibration very challenging (Amini 2014). Recent alternative approaches have been proposed to incorporate 4DS data into history-matching procedures, avoiding the use of petro-elastic models. One possibility is the use of binary images to represent the dynamic changes to be matched (Jin *et al* 2012, Tillier *et al* 2013, and Obidegwu *et al* 2015). Other examples are works that use parameterization of seismic data in terms of front propagation (Trani *et al* 2012, and Leeuwenburgh and Arts 2014).

History matching is an inverse process that can be solved by several methods, including optimization procedures or sampling algorithms (Maschio and Schiozer 2016). Currently, probabilistic procedures that generate several possible model realizations are preferred as they allow proper handling of uncertainties. Examples of this type of approach are the Kalman filter (Aanonsen *et al* 2009), the ES-MDA (Emerick 2016), and the probabilistic procedures using discrete Latin Hypercube (DLHC) sampling proposed by Maschio and Schiozer (2016), Avansi *et al* (2016), and Almeida *et al* (2017).

The works of Maschio and Schiozer (2016), Avansi *et al* (2016), and Almeida *et al* (2017) present a similar general history-matching methodology, where DLHC is used within an iterative procedure to gradually update the probability density function (pdf) of the attributes based on the models that present the lowest data misfit. The differences between these works concern the implementation of specific steps, such as the procedure to update attributes, and how to update petrophysical properties (geostatistical images) presented by Avansi *et al* (2016) and Almeida *et al* (2017). The three works demonstrated the robustness of this methodology by applying it to different synthetic datasets. Besides being robust, it is simple to implement. The present work applies this history-matching methodology to a segment of a real field, using well data. We also show the incorporation of 4DS data, using binary images, into this history-matching process. The application is performed with the available data from the G-segment of the Norne benchmark case. Despite having only two wells in the G-segment (up to 2006), this part of the field experienced intensive production activity caused by producer depletion and the water injector. Consequently, strong 4D signals can be observed, resulting from fluid changes (water flooding, gas exsolution and dissolution) and pressure changes (pressure build up). While interpreting 4D anomalies related to fluid changes is uncertain, the softening effect caused by pressure build up is clearer to interpret. Therefore, this work uses binary images to match the pressurized zones. Note that the petro-elastic modeling for this field is very

uncertain, especially the calibration of pressure sensitivity, which motivated the use of binary images in this case. Also, the history matching for these two wells is not simple as the intra-segment connectivity is complex due to lithology change and a complex fault system (Huang *et al* 2013).

This work presents the application of the aforementioned probabilistic history-matching methodology (Maschio and Schiozer 2016) with real data, incorporating a seismic objective function (OF) using binary images to match pressurized zones.

2. Methodology

2.1. History-matching procedure

This work applies the history-matching methodology presented by Maschio and Schiozer (2016), a probabilistic, iterative procedure that gradually updates the pdf for the attributes based on models that present the lowest data misfit. Although the applied procedure is very similar to ‘Method 3’ of the aforementioned methodology, there are some adaptations, such as the addition of the seismic OF, further explained below.

The general workflow comprises five steps. A brief explanation of each step is given below, for detailed information refer to Maschio and Schiozer (2016).

- Step 1: data parameterization. In this step we map the most important uncertain attributes to be considered in the matching procedure. All the uncertain attributes are considered discretely, so in this step, they are discretized on a given number of levels to be used in the following step.
- Step 2: generation of model samples using DLHC with geostatistical realizations (DLHG). DLHG is an extension of the DLHC that incorporates the Geostatistical realizations in the sampling procedure. See Schiozer *et al* (2017) for more details.
- Step 3: run flow simulations for the set of generated models.
- Step 4: compute the normalized misfit of all data considering well data, or well data and 4DS data.
- Step 5: select the best models according to the match quality using a correlation matrix and use these models to update the pdf for attributes.

If the stop criteria is reached the process is finished, otherwise we go back to the second step and generate new models using the updated pdf obtained in step 5. This process is repeated until the stop criterion is reached.

To allow full understanding of the results, steps 4 onwards are detailed in the next section.

2.2. Compute normalize misfit

This section describes how data misfits are computed in step 4.

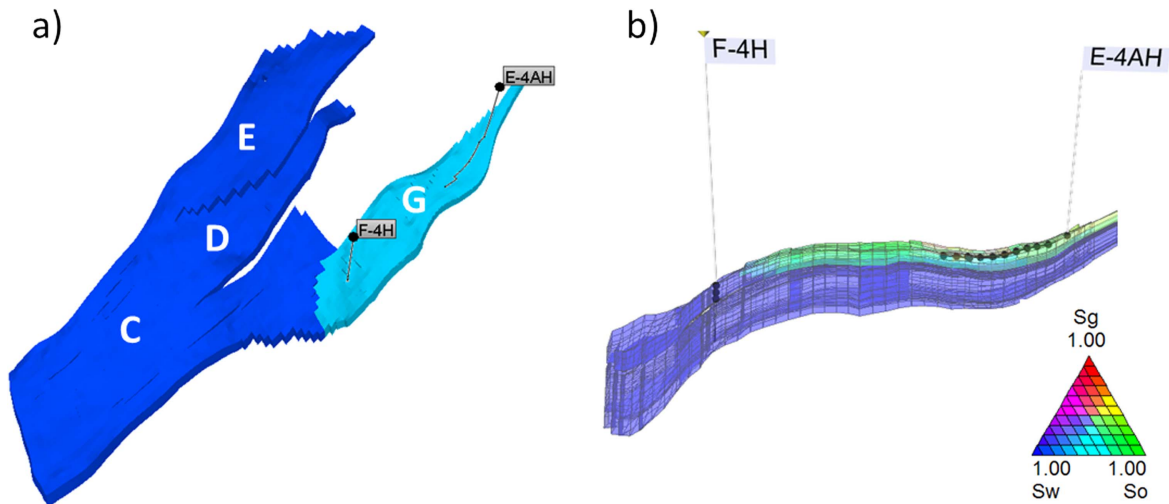


Figure 1. (a) Horst structure of the Norne field and its four segments (C, D, E, and G). The G-segment (focus of this work) is highlighted in light blue together with its two wells. (b) Cross sections showing the completions of producer E-4AH and injector F-4H. The ternary color scale shows the saturations at the moment the injector was drilled.

2.2.1. Well OF. Well data misfit is measured by a normalized quadratic distance indicator defined by several authors (Mesquita *et al* 2015, Avansi *et al* 2016, Maschio and Schiozer 2016, Almeida *et al* 2017) as the equations:

$$NQD = \frac{QD}{AQD} \tag{1}$$

being

$$QD = \sum_{i=1}^{N_{obs}} (Sim_i - Hist_i)^2 \tag{2}$$

and

$$AQD = \sum_{i=1}^{N_{obs}} (Tol * Hist_i + C_p)^2, \tag{3}$$

where Tol is the tolerance given by a percentage of the observed data (Hist), C_p is the constant used to prevent division by zero, Sim is the simulation result (such as oil rate) and N_{obs} is the number of points in the data series.

To evaluate the error distribution around the history data, we use the NQDS indicator, which includes the signal of the deviation through the linear deviation:

$$NQDS = \frac{LD}{|LD|} NQD, \tag{4}$$

where

$$LD = \sum_{i=1}^{N_{obs}} (Sim_i - Hist_i). \tag{5}$$

The NQDS indicator is an efficient indicator, enabling a quantitative evaluation of the models as well as a visual evaluation of many OFs for several models simultaneously. The NQDS range of $[-1 + 1]$ represents an excellent matching quality, i.e., the simulated data provide values within the user defined tolerance (tol and C_p). Previous works

Table 1. Uncertain attributes and its corresponding value for each discrete level.

Attribute	Levels				
mpoA, mpoB, mpoC	1	1.1	1.2	1.3	1.4
mpeA, mpeB, mpeC	1	1.7	3	5	7.5
mAB, mBC	0	0.01	0.1	1	—
Faults transmissibility	0	0.1	1	—	—
KrPc	1	2	3	4	—

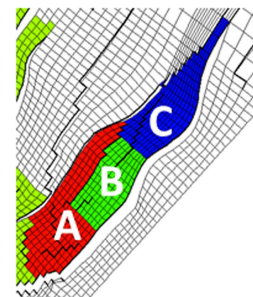


Figure 2. Three regions (A)–(C) used to apply multipliers of porosity and permeability.

(Mesquita *et al* 2015, Avansi *et al* 2016, Maschio and Schiozer 2016, Almeida *et al* 2017) suggest relaxing this range for complex cases, as having a set of models with all OFs (fluid rates and pressure) within the $[-1 + 1]$ limit is very difficult.

2.2.2. Seismic OF. 4DS data and the corresponding simulation results are converted to binary images, for comparison. Thus, instead of using the usual quadratic error, we use the methodology proposed by Tillier *et al* (2013) to measure the similarity between two binary images,

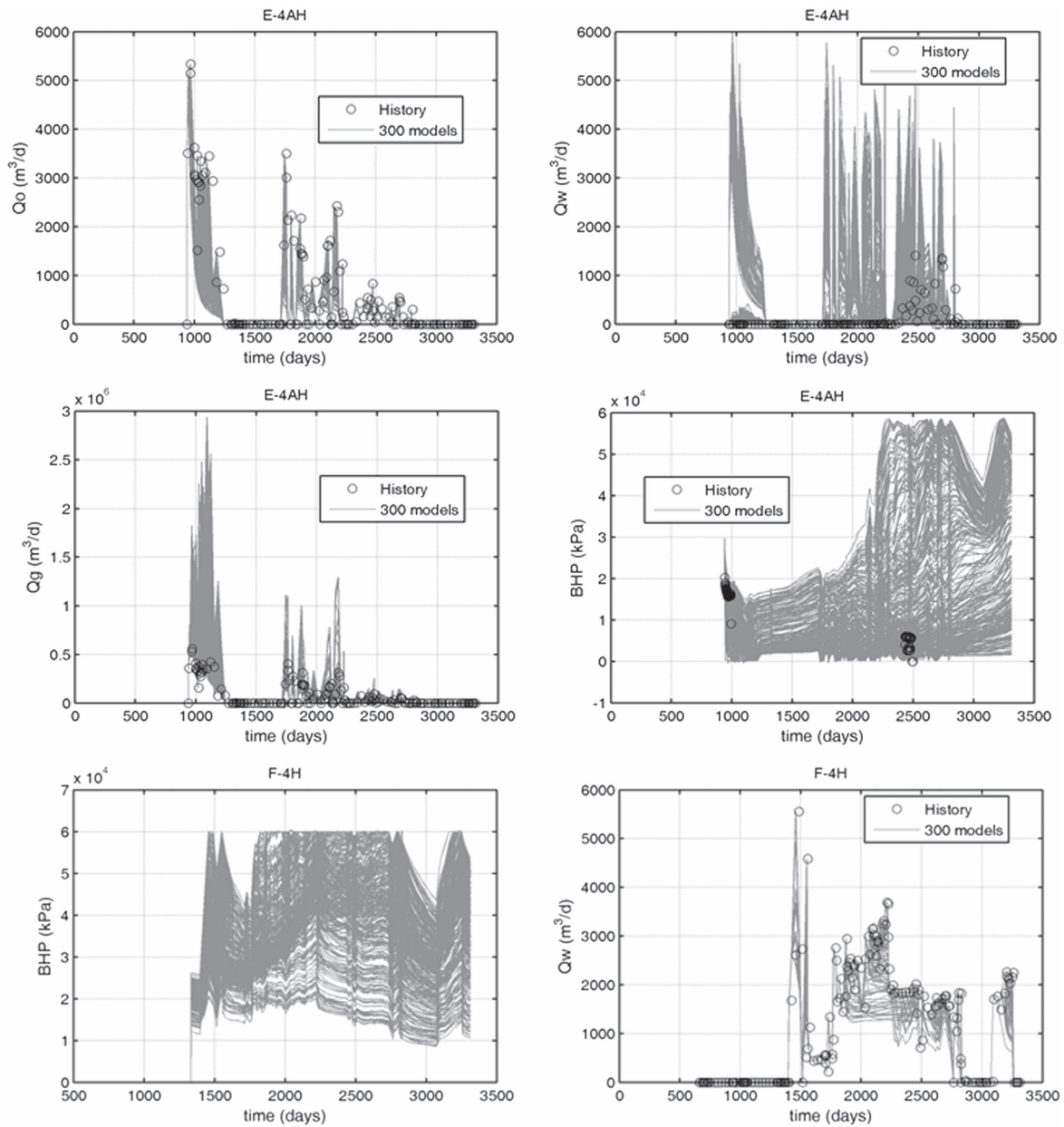


Figure 3. Well production curves for the initial set of 300 models and history data in black circles.

A and B, according to equation (6).

$$OF_{bin} = \frac{1}{2} \sum_{i=1}^N LDM(A, B)_i^2, \quad (6)$$

where LDM is the local dissimilarity map defined as

$$LDM(A, B) = |A_i - B_i| \max(DT(A)_i, DT(B)_i), \quad (7)$$

where DT(A) is the value of the distance transform of the image A at pixel i.

The seismic OF was normalized so that all misfits (well and binary images) have the same magnitude. Through a visual inspection of the binary images, we set a maximum value of OF_{bin} so that the matching quality was considered acceptable. This maximum value (maxlim) was used to

normalize OF_{bin} . Therefore, the seismic OF is set as:

$$OF_{map} = OF_{bin} / \max \text{lim}. \quad (8)$$

Despite an exhaustive inspection to define this limit, future works could improve the definition of this normalization. Also note that, unlike NQDS, the OF_{map} is always positive.

It is worth mentioning that there is no limit concerning the number of seismic surveys to apply the seismic history matching (SHM) here proposed. Indeed, the methodology is very flexible to handle several surveys simultaneously.

2.3. Selection criterion and attribute updating

In step 5, we select a percentage of the best models to update the pdf of the attributes. There are different ways to rank and

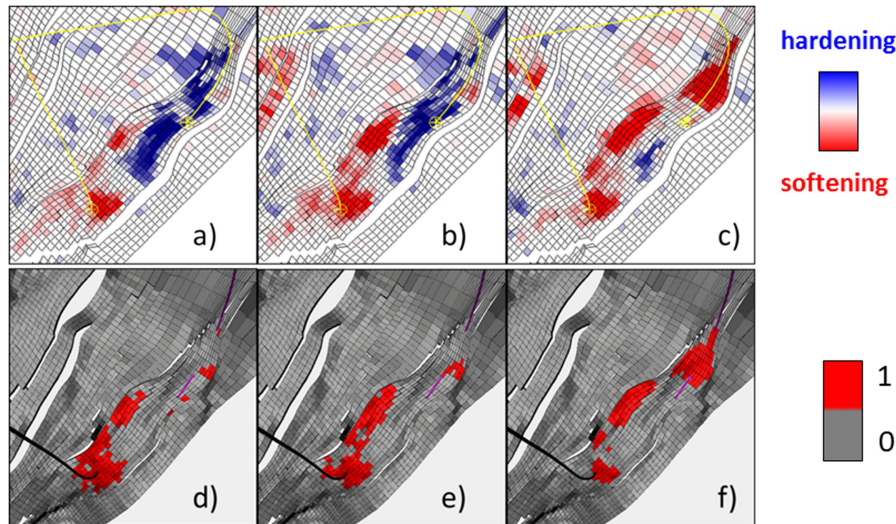


Figure 4. 4D seismic amplitude differences from surveys 2003-2001(a), 2004-2001(b) and 2006-2001(c), and respective binary images (d)–(f).

select the best models. The criterion used here is adapted from ‘Method 3’ described in Maschio and Schiozer (2016) and is summarized in the following steps.

- (i) Compute the correlation matrix. This matrix is used to capture the influence of each attribute on each individual OF (fluid rates and pressure for each well and 4DS data for each survey).
- (ii) For each attribute:
 - (a) Select the OFs with the highest correlations with the actual attribute.
 - (b) Find the NQDS and OF_{map} limits so that Nm models present all OFs, selected in step (ii)-a, within these limits. As proposed by Maschio and Schiozer (2016), the number of models selected (Nm) can vary during the process and should range from 5% to 15% of the total number of models.
 - (c) Build a histogram of the attribute using the Nm selected models.
 - (d) Generate the new pdf of the attribute by averaging the new histogram (step (ii)-c) with that of the previous iteration. This avoids the premature elimination of levels as proposed by Almeida *et al* (2017).
 - (e) If there are no OFs with high correlation with the actual attribute, then all OFs are used to update the pdf of this attribute.

The stop criterion based on previous works (Avansi *et al* 2016 and Almeida *et al* 2017) is to generate one hundred models with all OFs within the defined tolerance range.

2.4. Cases performed

The history-matching procedure was performed three times:

- Case well history matching (WHM): using only well data;
- Case SHM: using both well data and 4DS data;
- Case OSM (only seismic matching): using only 4DS data.

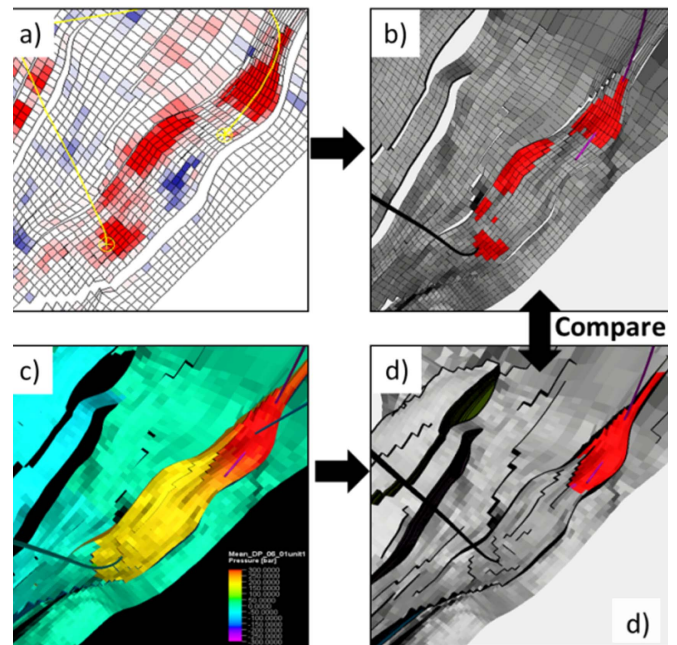


Figure 5. Scheme comparing seismic and simulation data. The similarity of the amplitude changes due to pressure build up (a) while the most pressurized zones from simulation (c) are measured by comparing the correspondent binary images (b) and (d).

For cases SHM and OSM, the 4DS data are incorporated as binary images. The image generation is discussed in the following sections.

3. Dataset description

The dataset used is from the Norne benchmark case organized by the Center of Integrated Operations in the Petroleum Industry (IO Center), the Norwegian University of Science

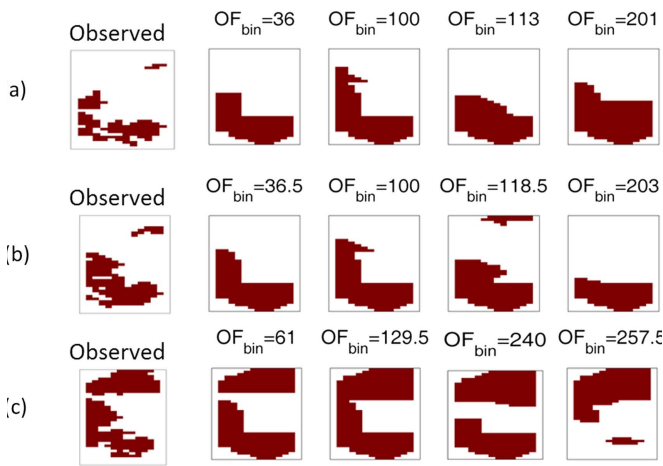


Figure 6. Examples of OF_{bin} values for: (a) S31, (b) S41, and (c) S61.

and Technology (NTNU), and Norne Field Operations (Statoil, ENI and Petoro). This dataset comprises real data, such as well logs, production history data (up to 2006), and seismic volumes (Rwechungura *et al* 2010). The Norne field is a 3×9 km horst structure located in the Norwegian Sea. It consists of two separate oil compartments (figure 1(a)), the Norne Main Structure (C, D and E-segments), containing 97% of the oil in place, and the Northeast Segment (G-segment). The field was discovered in 1991 and production started in 1997 (Statoil 2004). The simulation model used in this work has a total of 44 431 active cells defined in a corner point grid ($46 \times 112 \times 22$). It is a black oil model with 5 different equilibrium regions (each of them defined by different water-oil contact and gas-oil contact).

This work focuses on the G-segment (figure 1(a)). For this segment, the producing zone is the upper-most formation (Not formation) with an average thickness of 25–30 m, which was initially undersaturated. Two wells were drilled in this segment for the production period considered in this work (from 1997 to 2006): the producer E-4AH, drilled in the upper part; and the water injector F-4H, perforated downflank (figure 1(b)). Well E-4AH started producing in July 2000 and was closed in June 2001 due to lack of pressure. Well F-4H started water injection in September 2001 to provide pressure support to the producer that reopened in June 2002. The water injection caused a general pressure increase in the G-segment (Osdal *et al* 2006) resulting in strong 4D signals.

3.1. Initial set of models and well data

The uncertain attributes this work considers are: multipliers of porosity and permeability, the transmissibility of all faults inside the segment, relative permeability, and 200 sets of petrophysical images generated by Correa and Schiozer (2016), which included porosity, absolute permeability, and net to gross ratio. In each iteration, a set of 300 model realizations is generated.

All the attributes were considered in a discrete form assuming a prior uniform distribution. Table 1 shows the values assumed for each level for all the attributes, namely:

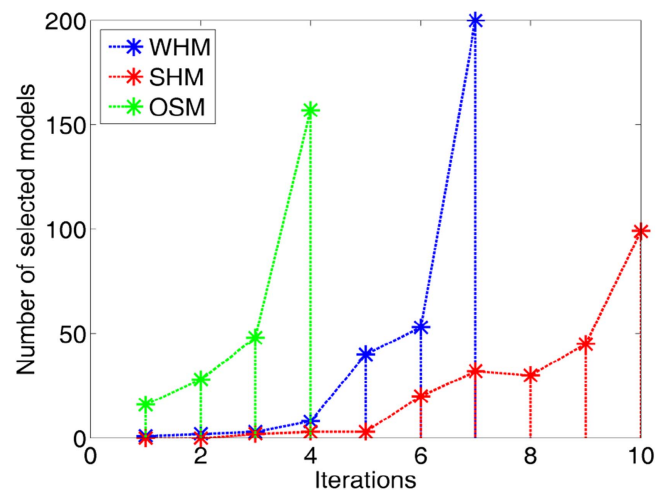


Figure 7. Evolution of three matching procedures for the number of selected models per iteration.

three multipliers of porosity (mpoA, mpoB and mpoC) defined according to the regions in figure 2, the corresponding horizontal permeability multipliers (mpeA, mpeB and mpeC); the transmissibility of the blocks between the regions A and B (mAB) and B and C (mBC); the transmissibility of all internal faults of the G-segment and four set of relative permeability and capillary pressure (KrPc).

The well history data available are oil, gas, and water rates for the producer E-4H and water rates for the injector F-4H. There is no pressure measurement for the injector, and the BHP (Bottom-hole pressure) for the producer is highly uncertain. Figure 3 shows well curves for the initial set of 300 models as well as the history data available. Note that the BHP of well E-4H presents several points concentrated at two specific times. As we are not confident about the reliability of these data, BHP was not included as an OF in the history-matching procedures. Thus, the well OFs are reduced to oil, gas and water production and water injection.

3.2. 4DS data

Four seismic surveys acquired in 2001, 2003, 2004, and 2006 were available. As the producing zone of the G-segment is located in the upper layers we extracted seismic amplitude maps along the top reservoir. Assuming the base survey as 2001, strong 4D signals are observed in the 4D differences of the three monitors, as seen in figures 4(a)–(c), showing the seismic amplitude differences transferred to the simulation model scale. From here on, we use the following nomenclature to refer to the seismic differences: S31 (2003-2001), S41 (2004-2001), and S61 (2006-2001). The softening anomalies (in red) are related to pressure build up due to water injection while blue anomalies are related to fluid changes, which can be either gas going back to solution or water flooding (Osdal *et al* 2006 and Santos 2017).

As the interpretation of the fluid anomaly is uncertain, we use only the anomalies related to pressure build up (red anomalies). After converting the 4DS data to the simulation

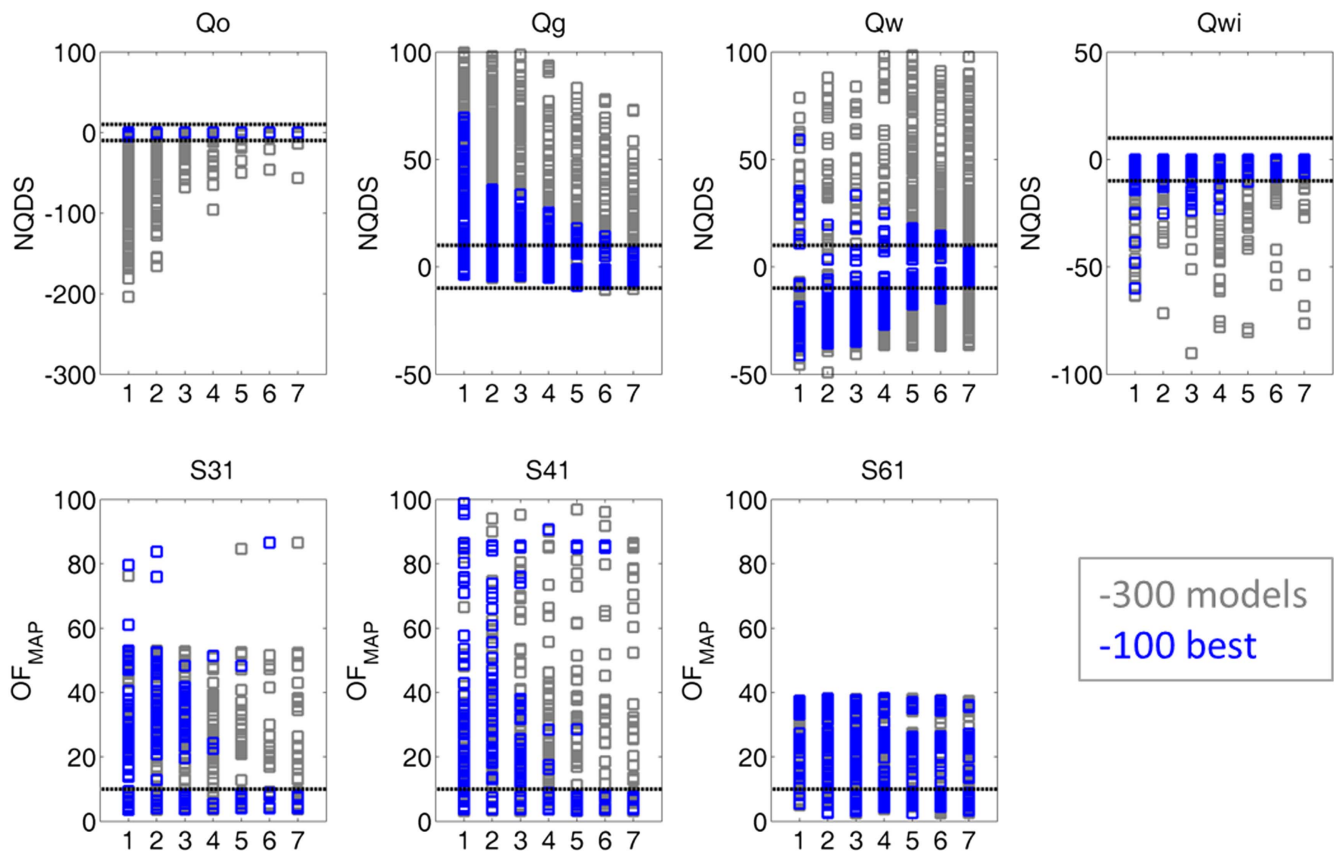


Figure 8. Results of WHM for each iteration. On the top row, well objective functions: NQDS of produced fluids (Q_o , Q_g , and Q_w) and injected water (Q_{wi}). On the bottom row, seismic objective functions: binary mismatch (equation (8)) considering the difference between surveys 2003-2001 (S31), 2004-2001 (S41), and 2006-2001 (S61). The seismic objective functions were not used in this procedure, but are shown here for comparison purposes. For all iterations, the 300 models are in gray and the 100 best models are in blue.

scale (figures 4(a)–(c)), they were converted to binary images by assigning the values of one, to the blocks with strong softening signals, and zero to the remaining blocks, as illustrated in figures 4(d)–(f). A cut-off was applied to the 4DS amplitude differences maps to define the cells strongest softening signals.

3.3. Comparing simulation and seismic data

For cases SHM and OSM, the binary maps generated from 4DS data (figures 4(d)–(f)) are compared with the pressure estimates from the simulation model. Figure 5 illustrates this process; not that no petro-elastic is required in this type of approach. The pore pressure estimates from simulation models are converted to binary images by applying a clustering technique (k-means). The pressure differences are computed using the dates of 4DS acquisitions (2003-2001, 2004-2001, and 2006-2001), then two clusters are generated (high and low pressurized zones). The blocks associated to the cluster of highest pressurized values are set to one, while the others are set to zero. It is worth mentioning that the pore pressure for all simulation models always increases from 2001, in the G-segment. Therefore all ΔP values were positive and using a two size cluster is suitable to get the shape of the most pressurized zone.

An average of the simulated pore pressure for the three layers of the producing zone of the G-segment (figure 1(b)) is considered to generate the binary maps. This choice was made based on the seismic resolution and the thickness of the G-segment (~25–30 m).

3.4. Tolerances and stop criteria

The parameter Tol in equation (3) was set as 5% for oil rate and injected water; these rates serve as boundary conditions in the simulator, so the tolerance is lower. Following previous works, we defined Tol = 15% for the other OFs (gas and water production).

As stated in previous works (Almeida *et al* 2017, Mesquita *et al* 2015, Avansi *et al* 2016, and Maschio and Schiozer 2016), $-1 < \text{NQDS} < 1$ represents excellent matching quality. As generating models within this limit is difficult, we set the range $[-10 + 10]$ to define good models.

Figure 6 shows some examples of OF_{bin} values. After a careful evaluation, we set the acceptance limits as $\text{OF}_{\text{bin}} < 100$ for S31 and S41, and $\text{OF}_{\text{bin}} < 240$ for S61. Therefore, to have $\text{OF}_{\text{map}} < 10$ (using the same magnitude as for NQDS), we defined maxlim (in equation (8)) equal to 10 for S31 and S41, and equal to 24 for S61.

With limits defined, the stop criteria for the three history-matching procedures are:

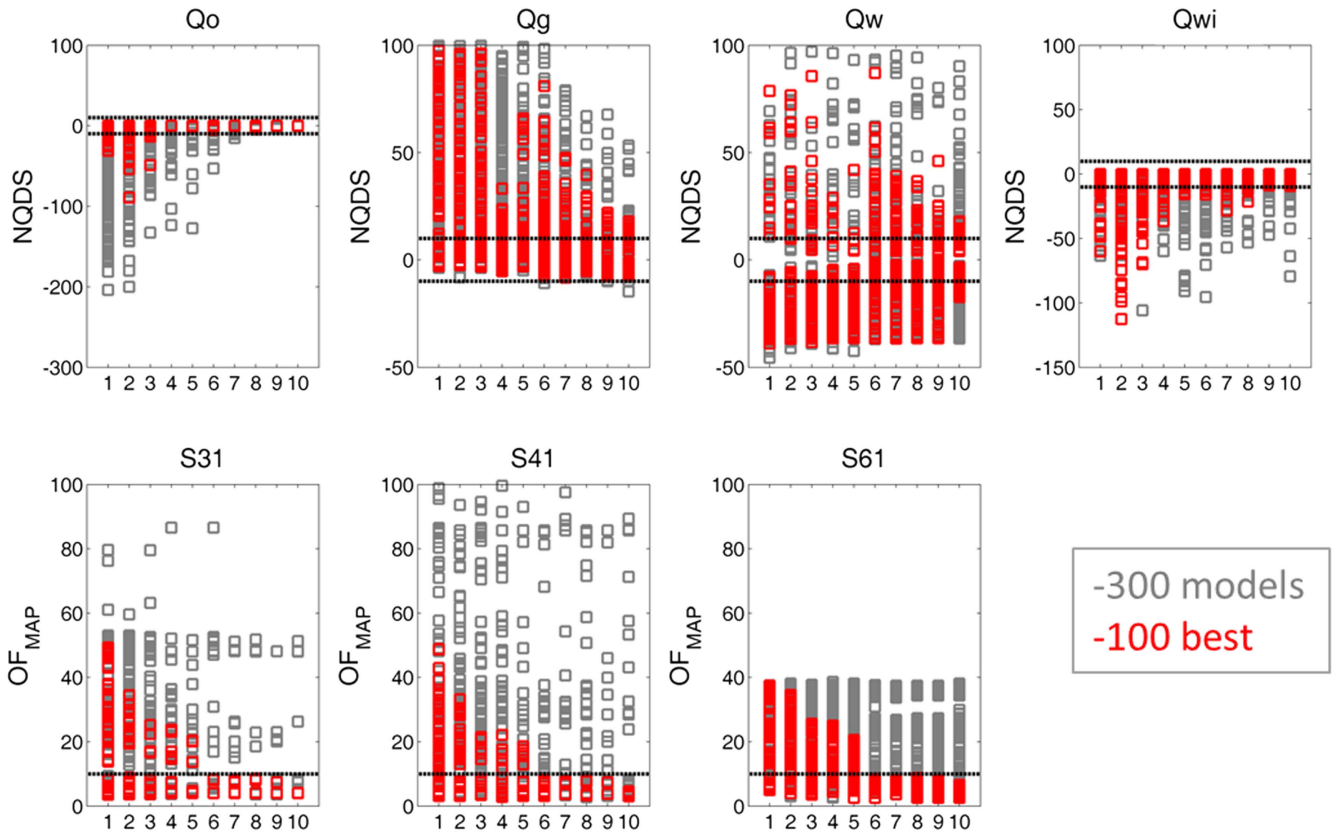


Figure 9. Results of SHM for each iteration. On the top row, well objective functions: NQDS of produced fluids (Q_o , Q_g , and Q_w) and injected water (Q_{wi}). On the bottom row, seismic objective functions: binary mismatch (equation (8)) considering the difference between surveys 2003-2001 (S31), 2004-2001 (S41), and 2006-2001 (S61). For all iterations the 300 models are in gray and the 100 best models are in red.

- WHM: around 100 models with $|NQDS| < 10$ for Q_o , Q_g , Q_w , and Q_{wi} ;
- SHM: around 100 models with $|NQDS| < 10$ for Q_o , Q_g , Q_w , and Q_{wi} , and $OF_{map} < 10$ for S31, S41, and S61.
- OSM: around 100 models with $OF_{map} < 10$ for S31, S41, and S61.

4. History-matching evolution

The three history-matching procedures WHM, SHM, and OSM required different numbers of iterations to reach the stop criteria. Figure 7 shows the evolution of the three procedures for the number of good models within tolerance for each iteration. WHM required seven iterations, achieving 200 models in the last iteration. SHM achieved 99 models in ten iterations, and OSM provided 160 models in four iterations. Note that initially, WHM and SHM presented no models fitting the selection criteria highlighting the challenge to match well data even for only two wells (4 well OFs).

Figures 8–10 show the data matching quality of the iterations for WHM, SHM, and OSM, respectively. Each point in these plots represents one model. For each iteration, we can see the mismatches for all 300 models in gray points. The black horizontal lines represent the acceptance range

(defined in section 3.4). To best visualize the evolution of the iterations, we also show the best 100 models from each iteration in blue, red, and green for WHM, SHM, and OSM, respectively.

Although the OF_{map} was not used in the WHM procedure, the values are shown for comparison purposes (figure 8); the same applies for well data displayed in figure 10 (OSM). An interesting observation for the WHM results is that for the two first monitors (S31 and S41), the models of the final iteration are within the OF_{map} tolerance. This indicates that adding these binary maps is unnecessary. This is not the case for the last monitor (S61), as only some models are within tolerance, as marked by the horizontal line.

For the SHM process, the best models improve gradually along the iterations for all considered OFs. These results support that the methodology satisfactorily generated models honoring not only well data, but also the expected binary images. Besides providing models within the acceptance range using the binary images, these models present the same well matching quality as those from the WHM procedure. This is evidenced by the production curves in figures 11(a)–(d) as well as by the histogram of the NQDS values of these final models presented in figure 12. The distribution of the gas rate misfits (figure 12(a)) are slightly better for the final models of SHM, as it presents more values concentrated closer to zero than the ones yielded from WHM. For the water

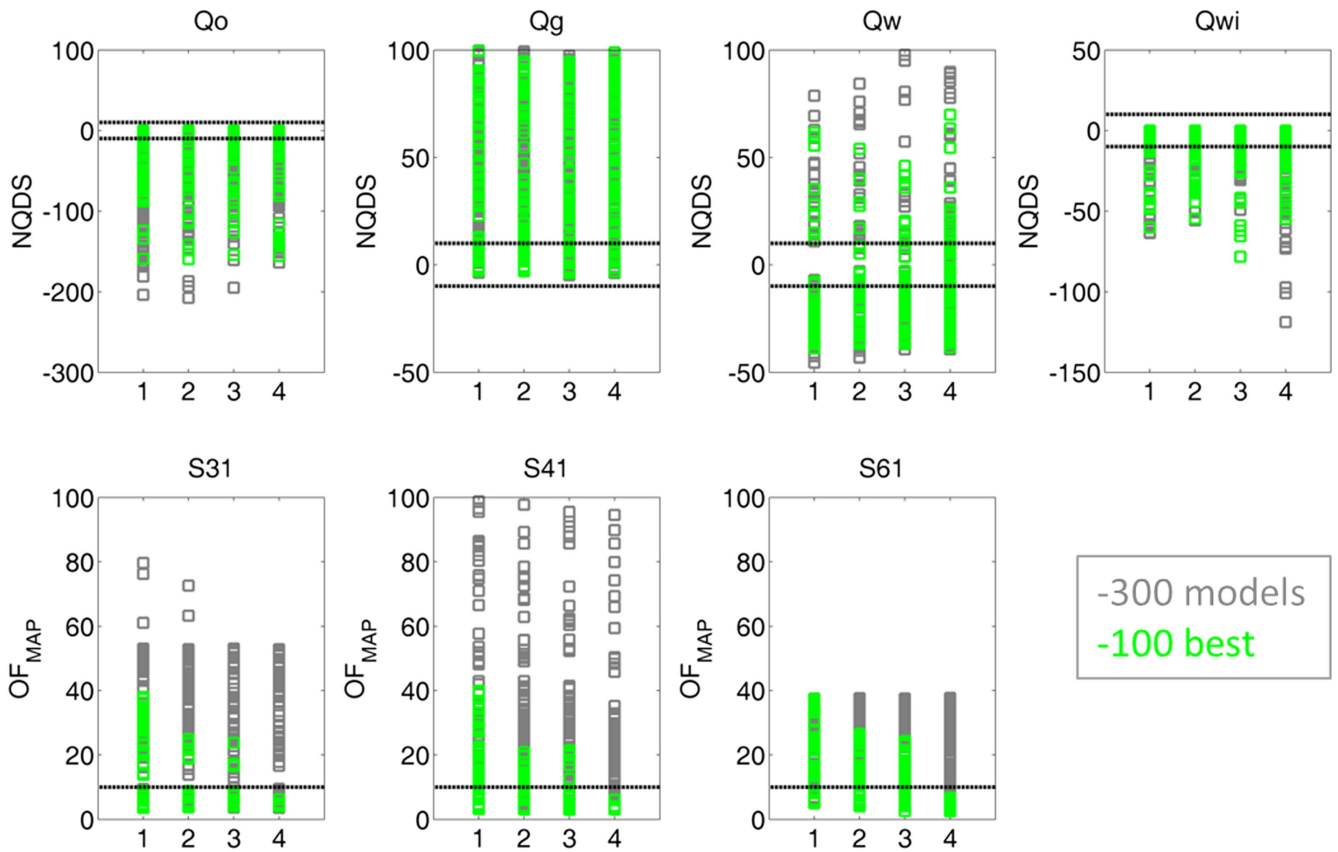


Figure 10. Results of OSM procedure for each iteration. On the top row well objective functions: NQDS of produced fluids (Q_o , Q_g , and Q_w) and injected water (Q_{wi}). On the bottom row seismic objective functions: binary mismatch (equation EE) considering the difference between surveys 2003–2001 (S31), 2004–2001 (S41), and 2006–2001 (S61). Well data were not used in this procedure; it is shown here for comparison purposes. For all iterations, the 300 models are in gray and the 100 best models are in green.

rate (figure 12(b)) the two distributions are very similar. Due to space limitation, figures 11 and 12 show only oil and water rates results, which are the most critical well OFs of this work.

The results of the OSM case (figures 10, 11(e), and (f)) show that the requirement of having the pressurized zones (as indicated in figures 4(d)–(f)) does not guarantee that these models are consistent with well history data. Indeed, this case provided the worst results.

Figure 13 shows the BHP curves for the three procedures, these results strongly indicate that the BHP measurements around 2500 days are incorrect. Also note that, according to Osdal *et al* (2006), a PLT in E-4AH in 2005 reported a pore pressure of 300 bar (marked with a yellow star) and we can see that both WHM and SHM provided BHP values around this value. Note that there is less scattering for SHM.

5. Image matching

As noted previously, matching the binary images for the time-lapse difference S61 was more challenging and so are analyzed in more detail. Figures 14 and 15 show the binary images from S61 for the best 25 models yielded from WHM and SHM, respectively, both of which provided the most

feasible models. The models of SHM better match the observed data, though some models from WHM also present good binary match, in agreement with the results of figures 8 and 9.

To analyze the differences of seismic attributes for the obtained models, we computed the impedance changes through a forward modeling using a petro-elastic model. Visual evaluation of the changes in acoustic impedance computed from the initial set of models revealed a behavior trend for these models for the three time-lapse differences, illustrated in figure 16. Similarly, the changes in impedances of the final models from WHM and SHM were qualitatively evaluated (observing positive and negative changes). This visual comparison revealed that there are two patterns frequently observed from the two cases, which are shown in figures 17 and 18. The impedance changes shown in figures 17 and 18 agree more closely with the observed amplitudes changes (figure 4) than the initial models (figure 16).

As stated by Huang *et al* (2013), the G-segment presents complex drainage patterns and pressure behavior, thus a perfect matching of 4DS behavior was not expected in this work. Despite this, we improved simulation models through matching well data and the pressurized zones. Future works could explore a more complete quantitative analysis of the

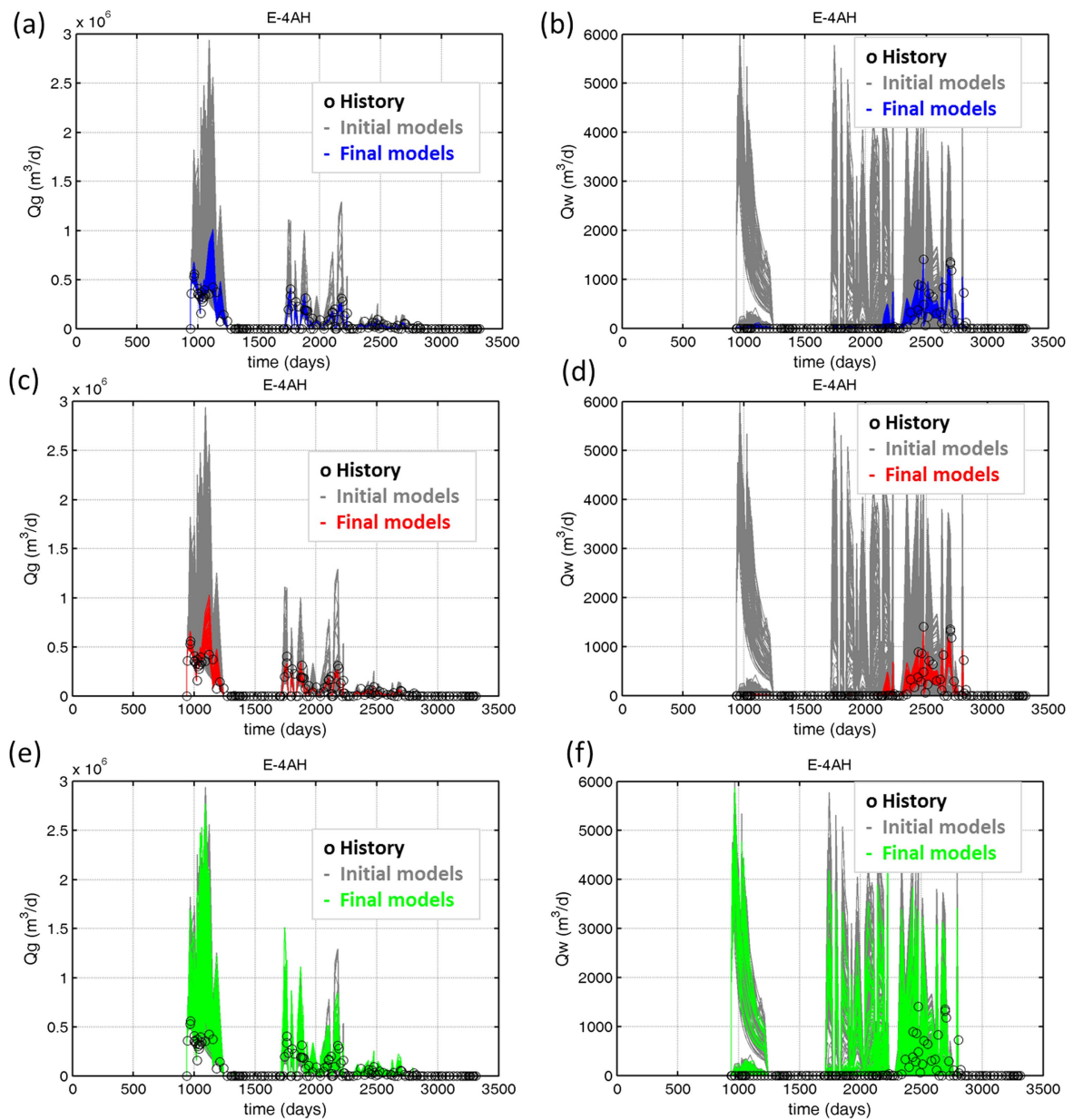


Figure 11. Left: gas rate curves for the cases WHM (a), SHM (c), and OSM (e). Right: water rate curves for the cases WHM (b), SHM (d), and OSM (f).

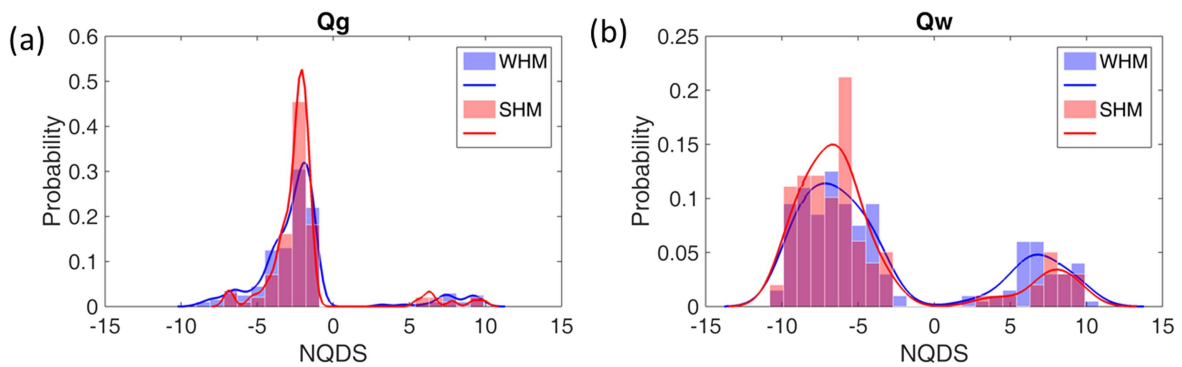


Figure 12. Histogram of the NQDS values of gas (a) and produced water (b) rates and their corresponding estimated density function. Blue and red indicated the final models yielded from WHM and SHM, respectively.

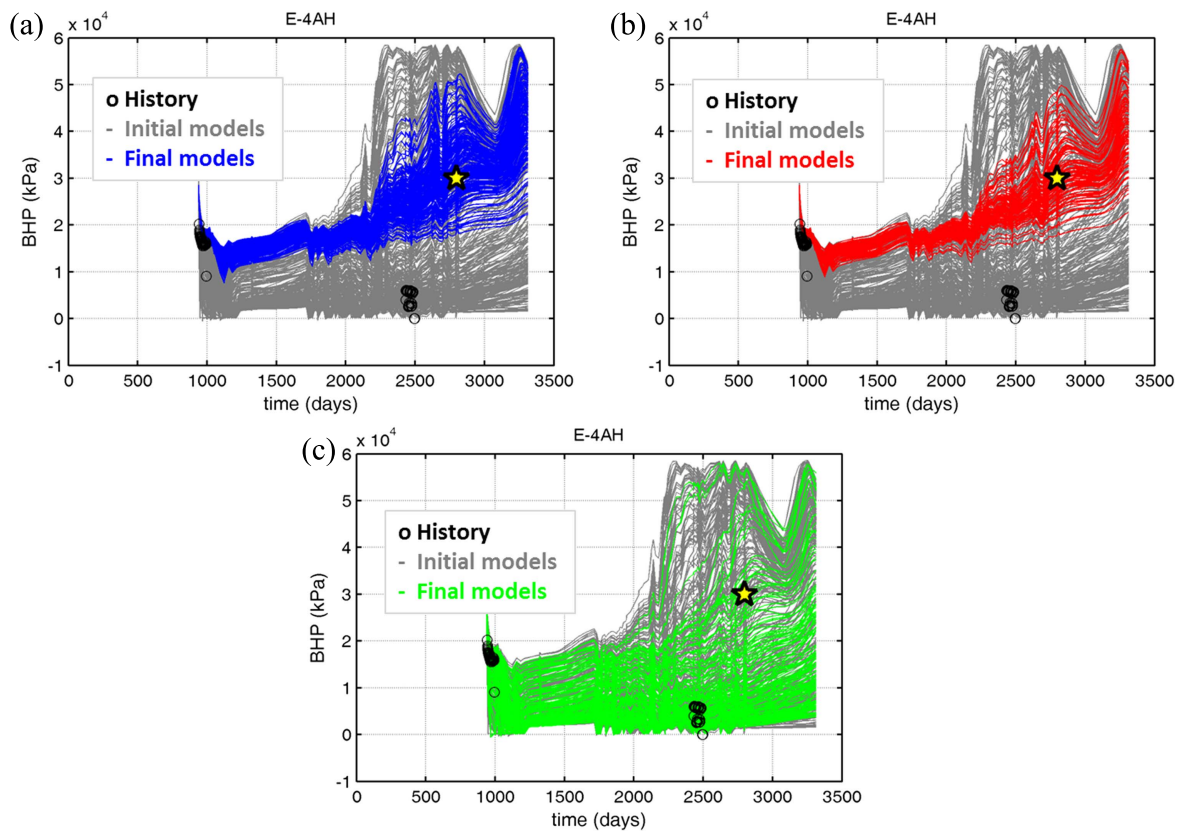


Figure 13. BHP curves for the three procedures: (a) WHM, (b) SHM, and (c) OSM. The yellow star indicates a pressure measurement from a PLT.

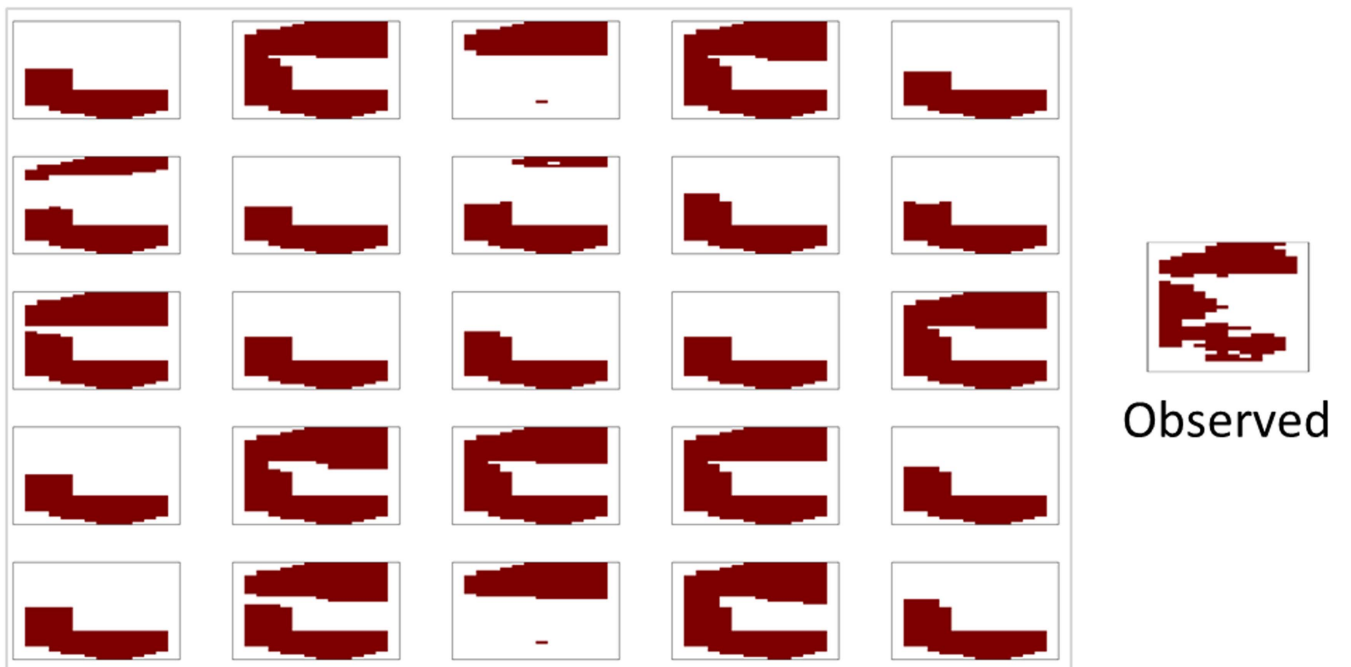


Figure 14. Binary images considering the time-lapse difference 2006-2001 for the 25 best models from WHM and the corresponding seismic binary image (on right).



Figure 15. Binary images considering the time-lapse difference 2006-2001 for the 25 best models from SHM and the corresponding seismic binary image (on right).

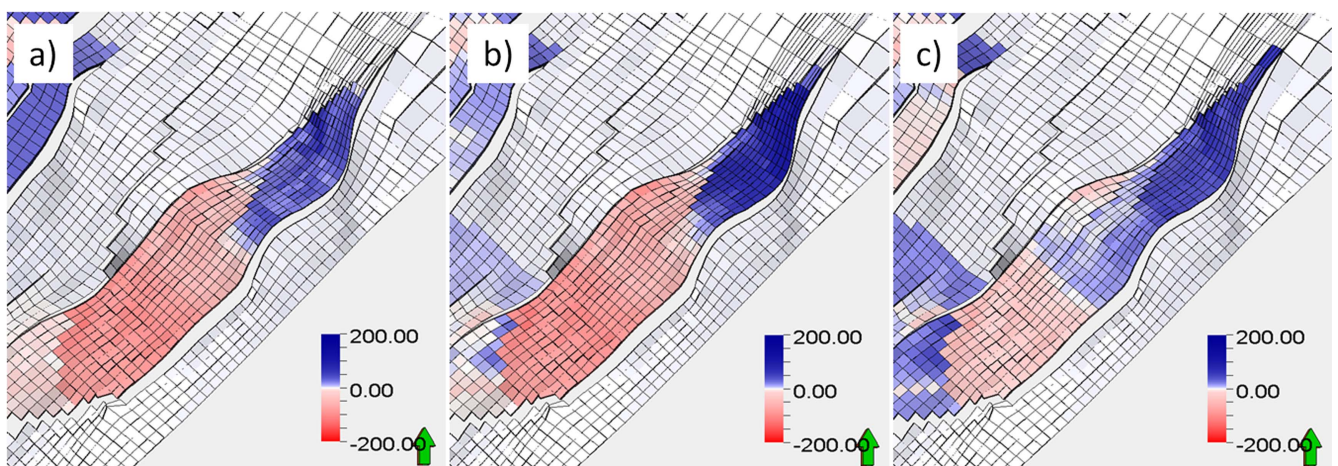


Figure 16. Example of typical behavior observed for changes in acoustic impedance computed from one of the initial simulation models (initial set figure 3) for the three time differences. (a) 2003-2001, (b) 2004-2001, and (c) 2006-2001.

impedance changes from the final matched models and should include the uncertainties related to the petro-elastic modeling.

6. Discussion

The pressure dependence of the seismic velocities is not linear. Therefore, to have a strong 4D signal (in this case, decreased impedance) as well as increased pressure, the pressure values at the time of monitoring must be higher than a threshold. This pressure threshold is defined through laboratory data (core plug measurements) as well as by matching synthetic and observed 4DS data (one of the most important calibration steps of the petro-elastic modeling). As we had no pressure measurements at the time of the seismic

surveys, we did not use any pressure constraints other than the pressurized zones defined by the binary images, but if these values are known, they can be used to constrain the cluster definition.

Using binary images to avoid the petro-elastic modeling might have a drawback, which is the lack of sensitivity to coupled effects (caused by simultaneous fluid and pressure changes) observed in 4DS signals. This is observed for S61, when figures 17(c) and 18(c) are compared to figure 4(c). Note that figure 4(c) presents a small blue region in the center, which is not observed in the computed impedances because the pressure effects override saturation effects. However, this issue is not present for S31 or S41 and the shape of pressurized zone is close to the observed shape (especially for figure 18(b)). The shape of the pressurized zones could likely

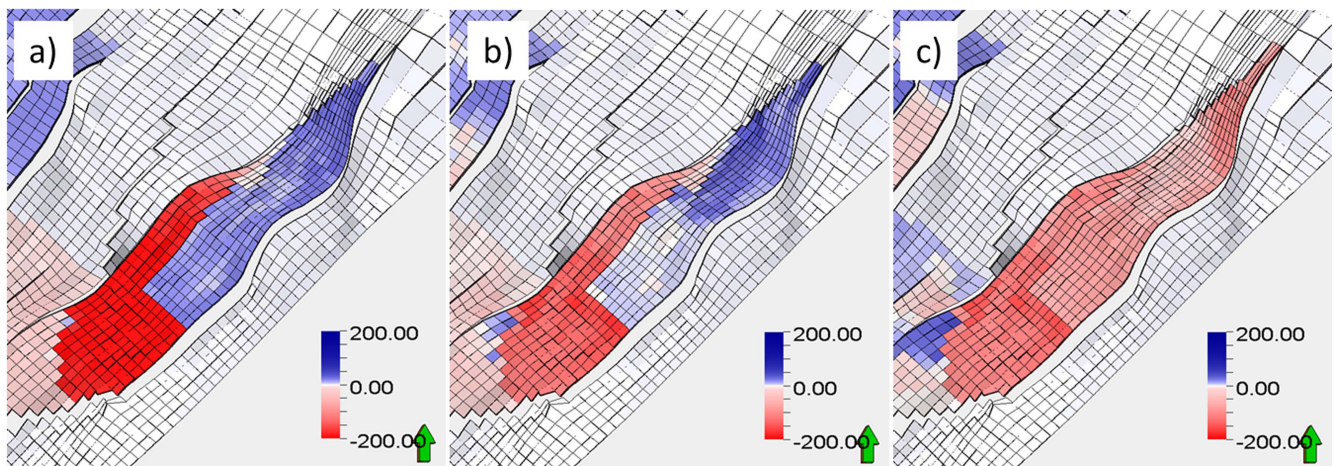


Figure 17. Example 1 of the typical behavior observed for changes in acoustic impedance computed from one of the matched simulation models from the WHM procedure for the three time differences. (a) 2003-2001, (b) 2004-2001, and (c) 2006-2001.

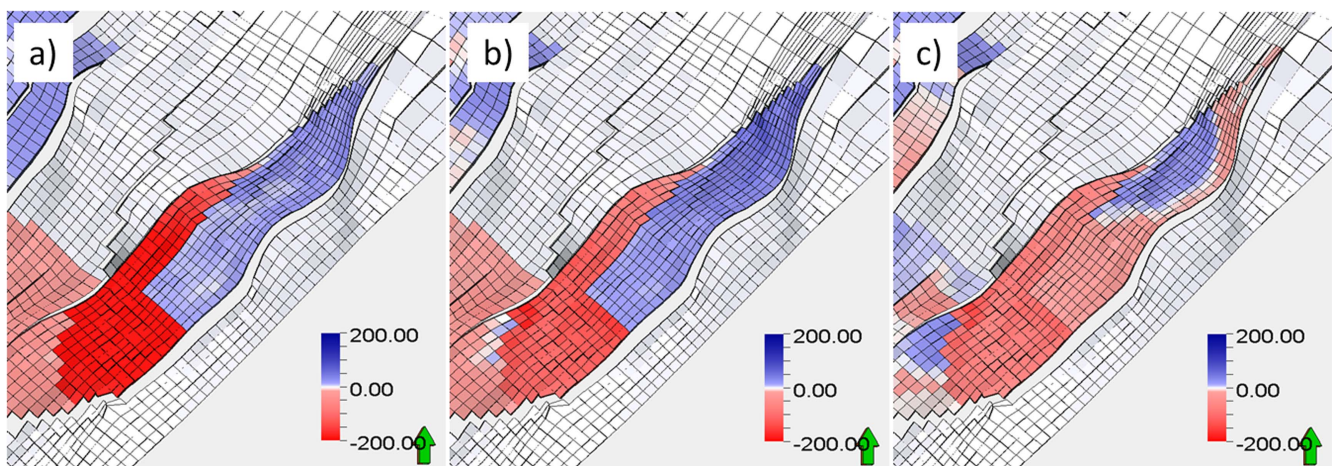


Figure 18. Example 2 of the typical behavior observed for changes in acoustic impedance computed from one of the matched simulation models from the SHM procedure for the three time differences. (a) 2003-2001, (b) 2004-2001, and (c) 2006-2001.

be improved through a more geologically consistent parameterization (not just by controlling the transmissibility of some model blocks), a suggestion for future studies. Another point that could be further evaluated is the performance of different metrics to compare images and how they impact the history matching process.

These results show that the successful use of binary images to avoid the petro-elastic model is case dependent. However, even for cases where the seismic response of the binary matched models do not correspond to the observed data (as shown here for S61), these binary matched simulation models can be used to improve the calibration of the petro-elastic model. Note that using the initial models to calibrate the petro-elastic model would be difficult as these models lack the expected dynamic behavior observed not only in the well history data, but also in the flow pattern suggested by 4DS interpretation.

7. Conclusions

This work presented the results of three history-matching procedures applied to the G-segment of the Norne benchmark case using a probabilistic history-matching methodology. The first procedure used only well data, the second procedure included 4DS data through the use of binary images where pressure estimations from simulation models are matched with 4DS amplitudes (softening anomalies), and the third procedure considered only binary images in the matching procedure. We found the history-matching methodology to be efficient using real data, and able to generate models that honor well and binary maps in few iterations. The methodology is flexible regarding the inclusion of new OFs, such as binary images, as shown here.

Results from the third procedure (OSM) presented very poor matches with well data. Therefore, only having a

pressurized zone at the location observed from the 4DS data is insufficient to generate feasible models (especially for this case with complex pressure behaviors). The other two procedures (WHM and SHM) generated models with a very similar matching quality for well data. The models from SHM presented pressure values (BHP) more concentrated around the expected value measured by a PLT, as well as they presented pore pressure changes according to the expected dynamic behavior (pressurized zones) observed on 4DS data. Evaluation of the impedances changes between the initial and final models of WHM and SHM procedures showed improvement with both sets of final models presenting improved dynamic behavior.

Given the complexity of the case study, we suggest dividing the problem into parts when using 4DS data to properly reduce uncertainties. An initial assessment can be made through some simplifications such as that presented here, with binary images. This first step will provide the means to improve the seismic modeling (a key step for successful SHM). Thus, in the second step, we would be able to run a more complete matching by adding the seismic attributes to the process to ensure a proper reduction of uncertainties.

Acknowledgments

This work was carried out in association with the ongoing project registered as BG-07 'Reduction of uncertainties through the incorporation of 4D seismic data in the modeling of the reservoir' (UNICAMP/BG Brazil/ANP) funded by BG E&P Brasil Ltda. (Shell Brasil Petróleo Ltda. Subsidiary) under the ANP R&D levy as 'Investment Commitment to Research and Development'. The authors thank UNISIM, CEPETRO and UNICAMP for supporting this work and Schlumberger and CMG for software licenses. We also would like to thank Statoil (operator of the Norne field) and its license partners ENI and Petoro for the release of the Norne Field data. Further, the authors acknowledge the Center for Integrated Operations at NTNU for cooperation and coordination of the Norne Cases. The view expressed in this paper are the views of the authors and do not necessarily reflect the views of Statoil and the Norne license partners.

References

- Aanonsen S I, Nævdal G, Oliver D S, Reynolds A C and Vall'es B 2009 The ensemble Kalman filter in reservoir engineering—a review *SPE J.* **14** 393–412
- Almeida F, Davolio A and Schiozer J D 2017 Methodology to systematically reduce uncertainty assimilating quantitatively 4D Seismic and well data in a probabilistic and multi-objective history matching *Proc. SPE Annual Technical Conf. and Exhibition (San Antonio, Texas, 9–11 October)* SPE-187081-MS
- Amini H 2014 A pragmatic approach to simulator-to-seismic modeling for 4D seismic interpretation *PhD Thesis* Heriot-Watt University
- Avansi D G, Maschio C and Schiozer J D 2016 Simultaneous history-matching approach by use of reservoir-characterization and reservoir-simulation studies *SPE Reservoir Eval. Eng.* **19** 694–712
- Correia G G and Schiozer D J 2016 Reservoir characterization using electrofacies analysis in the sandstone reservoir of the Norne Field (offshore Norway) *Pet. Geosci.* **22** 165–76
- Emerick A A 2016 Analysis of the performance of ensemble-based assimilation of production and seismic data *J. Pet. Sci. Eng.* **139** 219–39
- Huang Y, Alsos T, Sørensen H M and Tian S 2013 Proving the value of 4D seismic data in the late-life field—case study of the Norne main field *First Break* **31** 57–67
- Jin L, Weber D, van den Hoek P, Alpak F O and Pirmez C 2012 4D Seismic history matching using information from the flooded zone *First Break* **30** 55–60
- Landa J L and Kumar D 2011 Joint inversion of 4D Seismic and production data *Proc. SPE Annual Technical Conf. and Exhibition (Denver, Colorado, 30 October–2 November)*
- Landrø M 2001 Discrimination between pressure and fluid saturation changes from time-lapse seismic data *Geophysics* **66** 836–44
- Leeuwenburgh O and Arts R 2014 Distance parameterization for efficient seismic history matching with the ensemble Kalman filter *Comput. Geosci.* **18** 535–48
- Maschio C and Schiozer D J 2016 Probabilistic history matching using discrete Latin Hypercube sampling and nonparametric density estimation *J. Pet. Sci. Eng.* **147** 98–115
- Mesquita F, Davolio A and Schiozer J D 2015 A systematic approach to uncertainty reduction with a probabilistic and multi-objective history matching *Proc. EUROPEC 2015 (Madrid, Spain, 1–4 June)* SPE-174359-MS
- Obidegwu D, Chassagne R and MacBeth C 2015 Seismic assisted history matching using binary image matching *Proc. EUROPEC 2015 (Madrid, Spain, 1–4 June)* SPE-174310-MS
- Osdal B, Husby O, Aronsen H, Chen N and Alsos T 2006 Mapping the fluid front and pressure buildup using 4D data on Norne field *Leading Edge* **25** 1134–41
- Rwechungura R, Suwartadi E, Dadashpour M, Kleppe J and Foss B 2010 The Norne field case—a unique comparative case study *SPE Intelligent Energy Conf. and Exhibition (Utrecht, Netherlands, 23–25 March 2010)* SPE 127538
- Santos J M 2017 Semi-quantitative 4D Seismic interpretation integrated with reservoir simulation: application to the Norne Field *MSc Dissertation* University of Campinas
- Schiozer D J, Avansi G D and Santos A A S 2017 Risk quantification combining geostatistical realizations and discretized Latin Hypercube *J. Braz. Soc. Mech. Sci. Eng.* **39** 575–87
- Statoil 2004 Annual reservoir development plan/Norne field *Report*
- Tillier E, Da Veiga S and Derfoul R 2013 Appropriate formulation of the objective function for the history matching of seismic attributes *Comput. Geosci.* **51** 64–73
- Trani M, Arts R and Leeuwenburgh O 2012 Seismic history matching of fluid fronts using the ensemble Kalman filter *SPE J.* **18** 159–71
- Trani M, Arts R, Leeuwenburgh O and Brouwer J 2011 Estimation of changes in saturation and pressure from 4D seismic AVO and time-shift analysis *Geophysics* **76** C1–17
- Tura A and Lumley D E 1999 Estimating pressure and saturation changes from timelapse avo data *69th Int. Exposition and Annual Meeting, SEG Expanded Abstracts* pp 1655–8